IRRADIATION RESISTANCE ESTIMATION METHOD BY CRYSTAL LATTICE DISTORTIONS FAST CALCULATION FOR NI, CoCrFeNi AND CoCrFeMnNi FCC-ALLOYS

V.V. Uglov,[1,2,] N.A. Stepanjuk,[1] & S.V. Zlotski[1]*

[1]*Belarusian State University, Minsk, 220030, Belarus*

[2]*National Research Tomsk State University, Tomsk, 634050, Russia*

*Address all correspondence to: V.V. Uglov, Belarusian State University, 4 Nezavisimosty Ave., Minsk, 220030, Belarus; Tel.: +375293885131, E-mail: uglov@bsu.by

Original Manuscript Submitted: 5/18/2022; Final Draft Received: 6/3/2022

Bulk materials, pure Ni, CoCrFeNi, and CoCrFeMnNi, were deposited by arc melting with subsequent cold-rolling till 85% thickness reduction and annealing at 1150°C. They were irradiated by 40 keV He^{2+} and 280 keV Kr^{14+} low-energy ions to the fluences of 2×10^{17} cm^{-2} and 5×10^{15} cm^{-2}, respectively. Estimation of the distortions in the alloys was by calculating the normalized distortion parameter, which tends to increase with the increment of alloy complexity and atomic radii mismatch. x-ray diffraction (XRD) and scanning electron microscopy (SEM) analysis showed a common superiority of CoCrFeNi over pure Ni in radiation resistance (less lattice deformation, no blistering). In both Ni and CoCrFeNi after ion irradiation, signs of tension microstress remained positive and the magnitudes showed similar responses, CoCrFeMnNi microstresses became compressive-negative; the dislocation density also showed decrease after Kr-irradiation compared with non-irradiation. Mn addition to the ternary alloy changed its behavior radically.Normalized distortion parameter calculation can be performed for quick simple comparative theoretical analysis comparison of the radiation resistance, but will not give full information about the difference between stoichiometries investigated.

KEY WORDS: *high-entropy alloys, ion irradiation, radiation resistance, crystal lattice distortions*

1. INTRODUCTION

Modern challenges in the fields of nuclear energy are concentrated greatly across the power and efficiency of nuclear facilities by increasing their working temperatures (Ye et al., 2015; Manzoni and Glatzel, 2020). Classical materials, such as steels (including austenitic), nickel, and other metal alloys with a binary base, face phase transformations and significant degradation of physical and mechanical properties at elevated temperatures, corroding when in contact with liquid coolants and some gases, and swelling under high doses of neutron irradiation (Li et al., 2021). They also may become brittle, which leads to the loss of exploitation capabilities in a very short time. Similar materials are required in mechanical engineering, since the current materials of power plants are incapable of long-term operation in a chemically aggressive environment at high temperatures, which is especially important when developing new jet engines or spacecraft elements (Ye et al., 2015; Son et al., 2021).

One of the most perspective classes of materials for the aims named above can be high-entropy alloys (HEAs) (Zhang et al., 2014; Yu et al., 2016; Koval et al., 2020). They are a new class of materials, attracting the interest of the scientists from the whole world. The vanguard

works on the theme of high-entropy alloys belong to Cantor et al. (2004) and Senkov et al. (2011).

HEAs can have a structure that differs from the structures of many homogeneous solid solutions. In some cases, they cannot be represented as a solid solution with a crystal lattice based on the lattice of one single element (Zhang et al., 2014; Ye et al., 2015). Elevated entropy of mixing the constituent elements reduces the Gibbs free energy of the system and thus increases the thermodynamic stability of the HEA. Considering the variety of multicomponent solid solutions that are theoretically possible, the creation of a HEAs with any properties may occur (Karati et al., 2019; Pacheco et al., 2019).

The self-healing effect of HEAs, marked by the authors of many studies on radiation resistance of this class of alloys, is also to be mentioned (Xea et al., 2015; Lu et al., 2018). This effect means the return of the alloy crystal lattice, close to the initial condition, during and after the irradiation, together with neutralizing irradiating-induced defects. Xea et al. (2015) suggested that, by establishing the correct working temperature regime, it is possible to make self-healing effect of the HEA constantly regenerate the structure of the alloy (Lu et al., 2018; Jones and Owen, 2020; Tian et al., 2021).

All of the above suggest HEAs as direct candidates for structural materials of nuclear power plants and power units of new generation aircraft (Song et al., 2021; Zhang et al., 2021).

High-entropy alloys perform a number of effects, known as "core effects of high-entropy alloys." They are: entropy effect (thermodynamic stability), cocktail effect (inheritance of pure elements properties), sluggish diffusion effect (defect kinetics features), and distortion effect (atomic radii mismatch) (Murty et al., 2014; Lee et al., 2020).

The role of particular elements in the alloy is governed by a cocktail effect and consists of straight dependence of solid solution structure and its properties on its elemental composition. Sluggish diffusion and distortion effects can be derived from the elemental composition and are usually considered the reason for increased radiation resistance of high-entropy alloys. Therefore, the estimation of lattice distortions can be a simple and quick estimation of radiation resistance of the material.

The most widespread, economically and physically convenient processes are HEAs based on transition 3d-metals or refractory metals (Rogachev, 2020). Nickel-containing HEAs with face-centered-cubic (FCC) structure show advanced radiation resistance in comparison with steel and nickel-based alloys (Koval et al., 2020).

The main aim of this study is to establish the existence or absence of the dependence between theoretical lattice distortion magnitude and ion radiation stability of the CoCrFeNi and CoCrFeMnNi FCC-alloys structures.

2. EXPERIMENTAL

The Ni, CoCrFeNi, and CoCrFeMnNi samples were obtained in Beijing Institute of Technology according to the procedure shown in Fig. 1. Technically pure (до 99,97%) metal powders were arc-melted in a high-purity argon atmosphere with sequent casting into a copper mold to get bulk ingots. After crystallization, the alloys were annealed in vacuum for 24 h under 1150°C with the aim to homogenize and spheroidize the grain structure of the samples. Then cold rolling to 85% thickness reduction took place and final annealing under 1150°C for 72 hours, having the same aims, as previous one.

All samples have linear dimensions of 5 × 5 × 1.5 mm and the shape of rectangular parallelepipeds.

The irradiation of the samples was performed in the Institute of Nuclear Physics' Astana branch (Kazakhstan) on DC-60 ion accelerator facility. The samples were irradiated with 40 keV He^{2+} ions till 2×10^{17} cm^{-2} and 280 keV Kr^{14+} ions till 5×10^{15} cm^{-2}. This research imi-

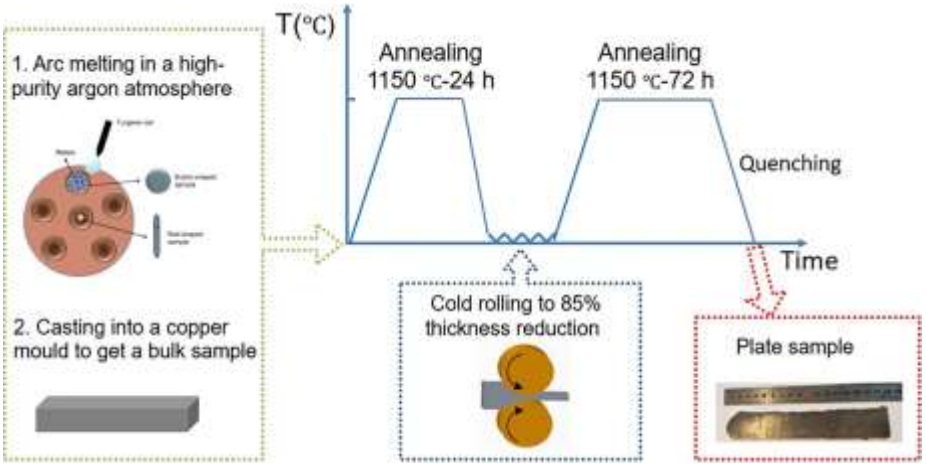

FIG. 1: Preparation procedure of pure Ni, CoCrFeNi, and CoCrFeMnNi alloy samples

tates the damage caused by low-energy fission products during neutron irradiation in nuclear facilities, leading to radiation swelling of the materials and modification of their physical properties.

Surface morphology analysis and analysis of elemental composition of samples were performed by scanning electron microscopy (SEM) and energy disperse X-ray spectroscopy (EDX) on ZEISS LEO 1455 VP scanning electron microscope, the images were obtained with acceleration voltage of 20 kV.

Phase analysis of the samples was carried out using X-ray diffraction method (XRD). XRD-spectra were obtained with Rigaku Ultima IV X-ray diffractometer using Cu K_α characteristic X-ray irradiation with wavelength of $\lambda = 0.1542$ nm in parallel X-ray beam geometry.

The results of the elemental compositions investigations for CoCrFeNi and CoCrFeMnNi non-irradiated samples are shown in Table 1. They prove that the samples with near-equiatomic elemental ratios.

The results of SEM investigations of the samples are presented in Figs. 2–4. It is evident that they have coarse-grained microstructure with grain size near 80 μm and 100 μm for CoCrFeNi and CoCrFeMnNi, respectively. The grains have a right polygonal shape with twinning regions, for all the systems. After irradiation, the surface morphology of HEAs remains the same as in nonirradiated samples, which confirms the microstructural stability of their radiation surface. Placed in the equivalent contents of irradiation, pure Ni, prepared the same way with HEAs,

TABLE 1: Elemental composition of CoCrFeNi and CoCrFeMnNi non-irradiated HEAs

i	c_i, in CoCrFeNi, at. %	c_i, in CoCrFeMnNi, at. %
Cr	25.8 ± 0.1	18.89 ± 0.1
Mn	0.0 ± 0.0	20.02 ± 0.1
Fe	25.0 ± 0.1	19.97 ± 0.2
Co	24.8 ± 0.1	20.74 ± 0.2
Ni	24.4 ± 0.1	20.38 ± 0.2

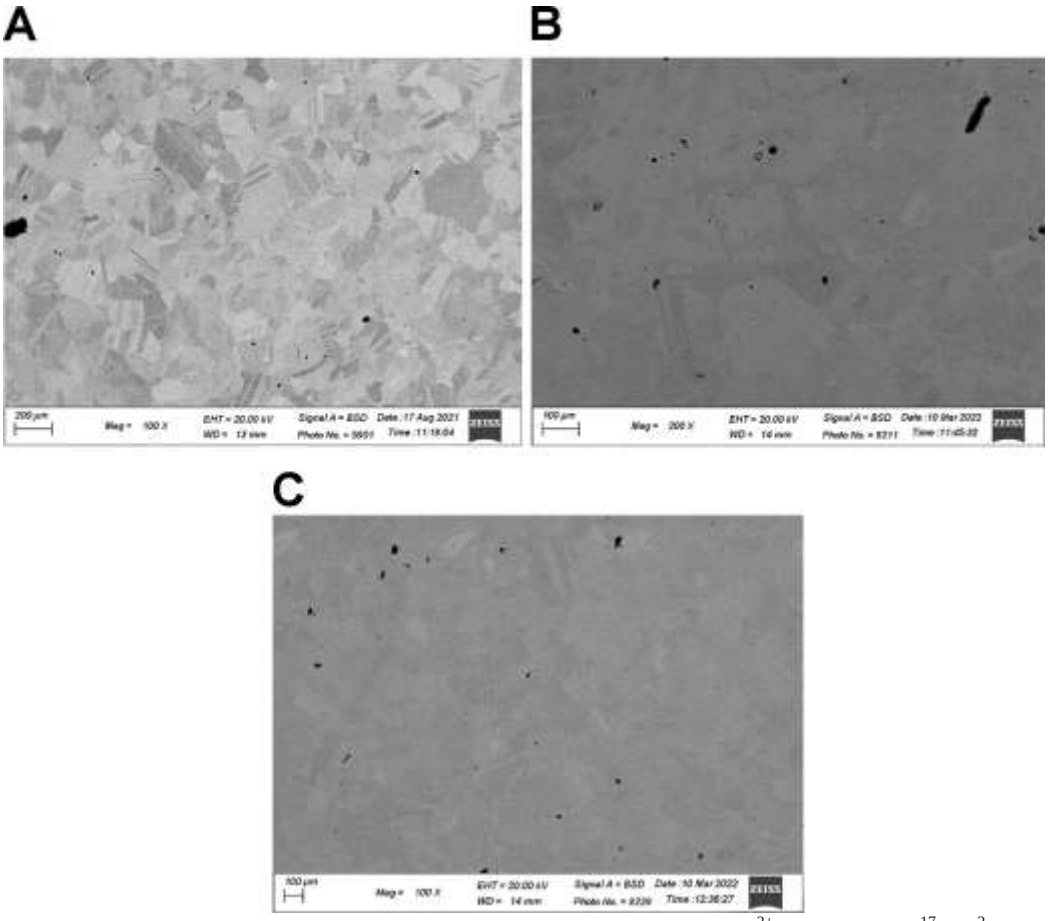

FIG. 2: SEM images of CoCrFeMnNi sample surface: (a) nonirradiated; (b) He^{2+}, 40 keV, 2×10^{17} cm^{-2}; (c) Kr^{14+}, 280 keV, 5×10^{15} cm^{-2}

shows significant blistering and surface erosion (Fig. 5), which is incorrect for complex alloys, where surface microstructure remains stable after ion irradiation.

XRD phase analysis (Figs. 5–7) of the samples shows the formation of single-phased systems, having FCC-type crystal lattice. The samples were analyzed on small incident angle (α = 1°), associated with penetration depth of nearly 300 nm according to the range of ions calculated using SRIM software in the materials mentioned.

Peak positions of HEAs are situated between the positions of FCC-lattices of all the pure constituent elements, which can be classified as substitutive solid solutions. Lattice constants of CoCrFeNi equals 0.3585 ± 0.0004 nm, 0.3574 ± 0.0004 nm for CoCrFeMnNi, and of 0.3511 ± 0.0004 nm for pure Ni.

After helium and krypton ion irradiation, the appearance of any additional peaks is not observed on XRD spectra. The diffraction reflex asymmetry (each of peak profile can be introduced as a combination of high narrow main peak and additional low wide peak with smaller angle gravity center) can be noticed for the ones irradiated with helium ions. Peaks have gravity center shifts after irradiation, which associated with change of the lattice parameters of all the materials after irradiation. The magnitudes of lattice constant increase equal (0.11 ± 0.01)% for CoCrF-

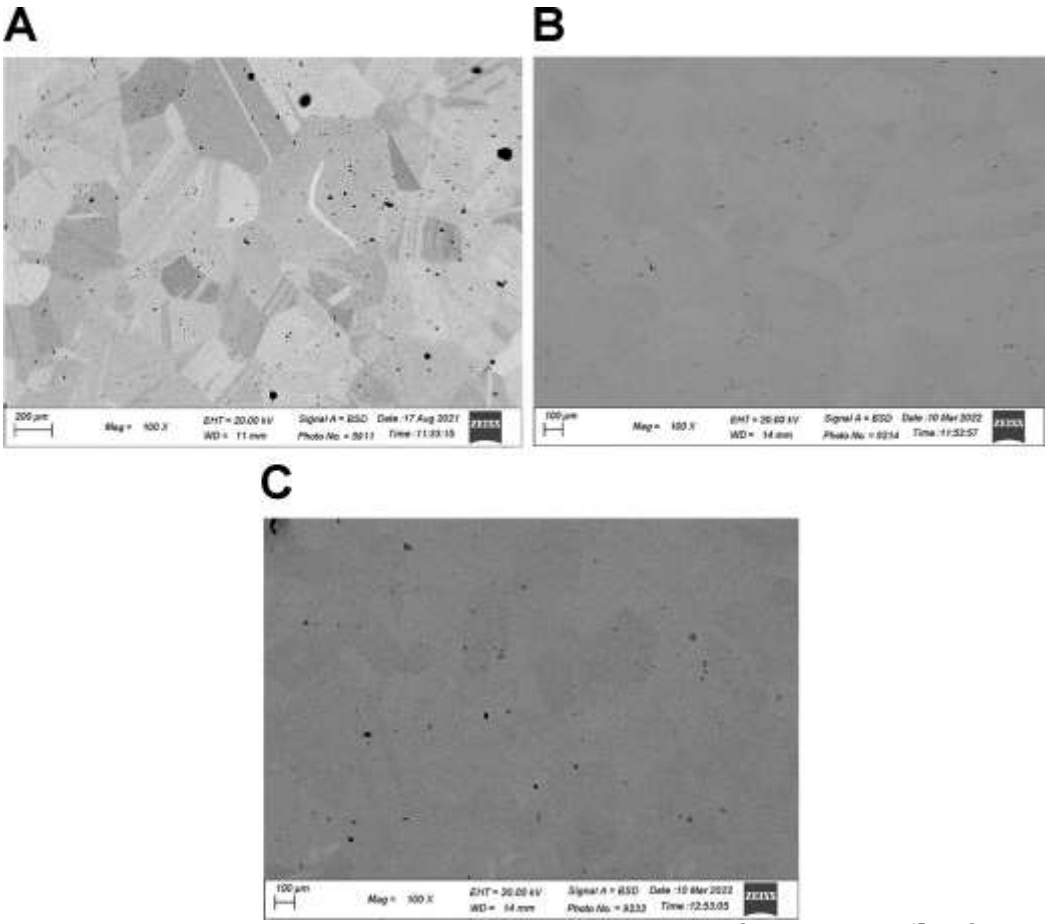

FIG. 3: SEM images of CoCrFeNi sample surface: (a) nonirradiated; (b) He^{2+}, 40 keV, 2×10^{17} cm^{-2}; (c) Kr^{14+}, 280 keV, 5×10^{15} cm^{-2}

eMnN, (0.22 ± 0.01)% for CoCrFeN, (0.34 ± 0.01)% for pure nickel. Krypton ion irradiation result in increase on (0.11 ± 0,01)% for CoCrFeMnNi, (0.11 ± 0.01)% for CoCrFeNi. In pure nickel, the decrease of lattice constant equals 0.04 ± 0.01% after krypton irradiation is observed. The phase composition of the HEAs is stable to irradiation, the deformation can be caused by creating more radiation-induced defects like gas–vacancy complexes.

The Williamson-Hall method was used to calculate crystalline size and microstrain in all the samples. Lattice strains were recalculated to microstress inside the sample grains, and crystalline size was used to estimate dislocation density (Fig. 8). All the samples react on krypton irradiation by decrease of tension microstresses, and the reaction on helium irradiation seem to increase the dislocation density significantly. It is interesting that CoCrFeMnNi decreased tension microstresses and transferred them into compressive stresses, while the most initially relaxed CoCrFeNi sample increased the magnitude of tension stresses much greater than pure Ni. It can be the result of elevated mobility of gas–vacancy complexes in CoCrFeMnNi.

Lattice distortion magnitude can be characterized with the help of physical quantity, such as lattice distortion parameter (Lee et al., 2020):

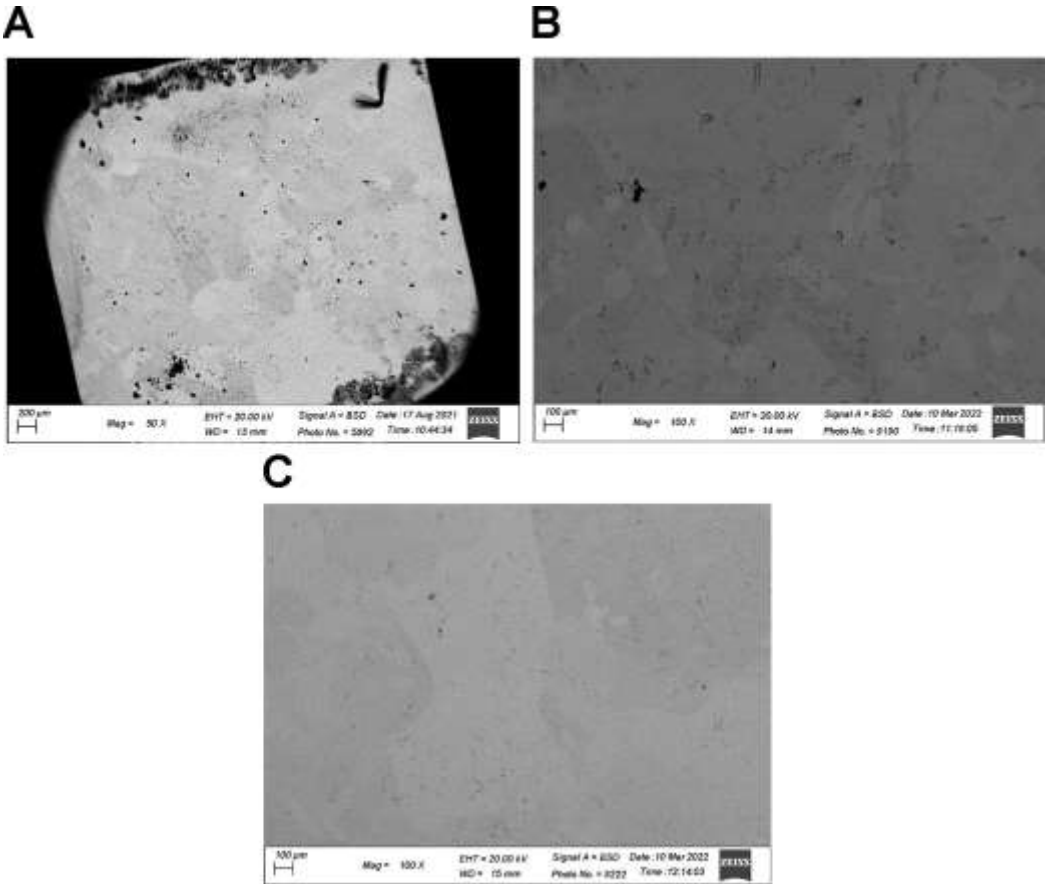

FIG. 4: SEM images of Ni sample surface: (a) nonirradiated; (b) He^{2+}, 40 keV, 2×10^{17} cm^{-2}; (c) Kr^{14+}, 280 keV, 5×10^{15} cm^{-2}

$$u^d = \sqrt{\sum_{i=1}^{n} \left(d_i^{3\phi\phi} - \bar{d} \right)^2}. \tag{1}$$

The physical meaning of lattice distortion parameter is a standard deviation of atom positions in solid solution lattice from their positions in ideal lattice without any distortions. The quantities in Eq. (1) are defined as the following:

$$\bar{d} = \frac{1}{n} \sum_{i=1}^{n} d_i^{3\phi\phi}, \tag{2}$$

$$d_i^{3\phi\phi} = c_i \sum_{i \neq j} d_{ij}, \tag{3}$$

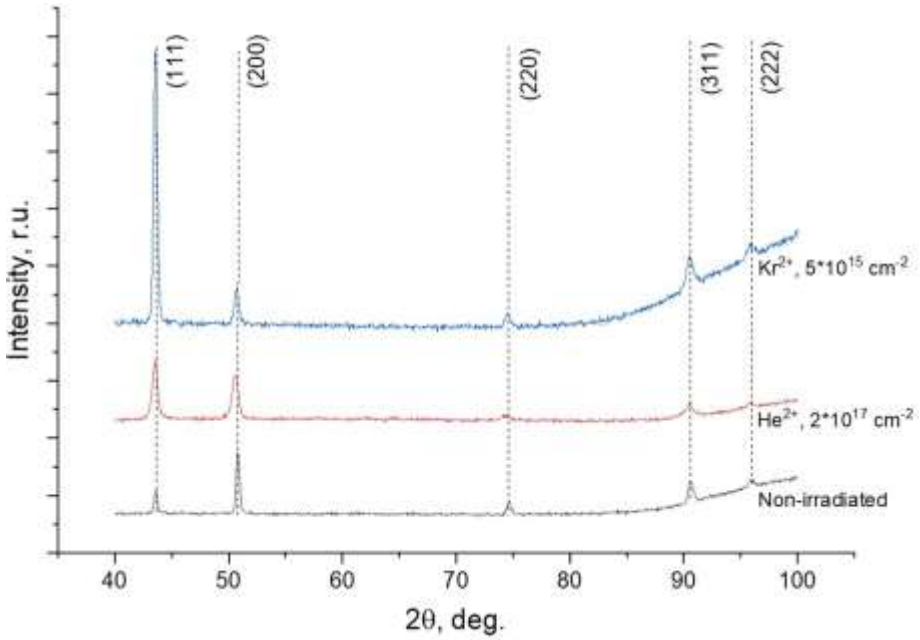

FIG. 5: XRD spectra of CoCrFeMnNi alloy samples, incident angle α = 1°: nonirradiated and irradiated with 40 keV He^{2+} ions, 2×10^{17} cm^{-2} and 280 кэВ Kr^{14+} ions, 5×10^{15} cm^{-2}

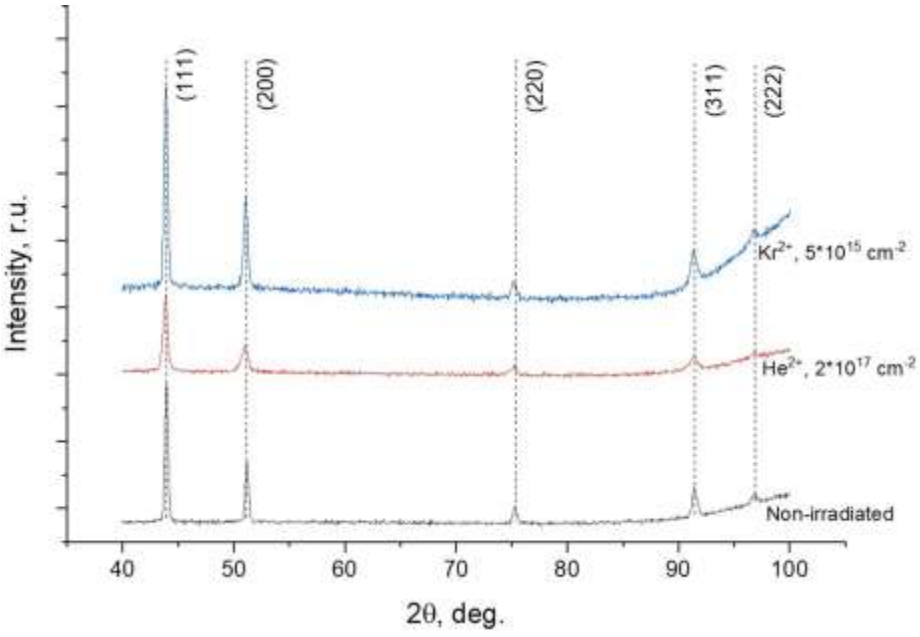

FIG. 6: XRD spectra of CoCrFeMn alloy samples, incident angle α = 1°: nonirradiated and irradiated with 40 keV He^{2+} ions, 2×10^{17} cm^{-2} and 280 кэВ Kr^{14+} ions, 5×10^{15} cm^{-2}

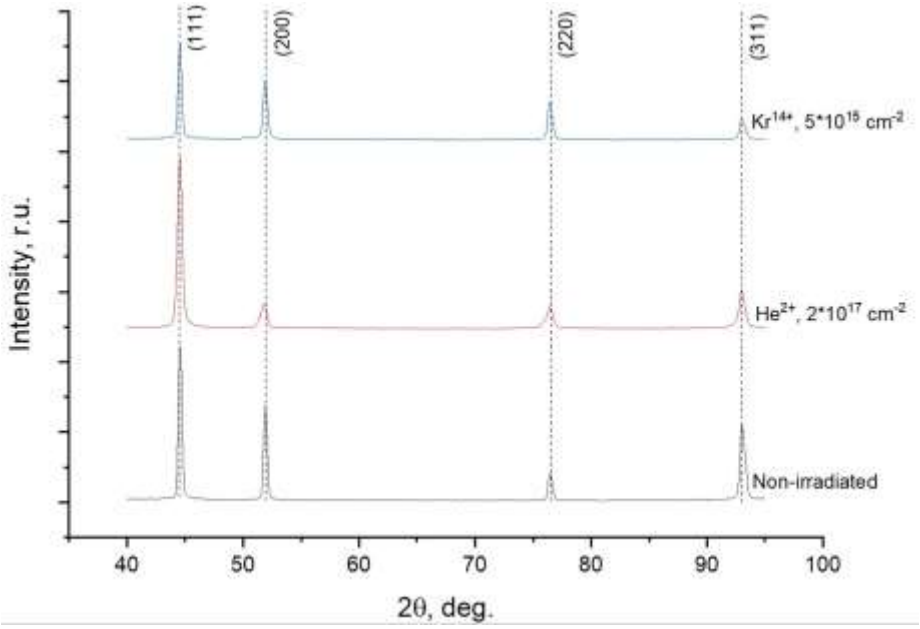

FIG. 7: XRD spectra of pure Ni samples, incident angle α = 1°: nonirradiated and irradiated with 40 keV He^{2+} ions, 2×10^{17} cm^{-2} and 280 кэВ Kr^{14+} ions, 5×10^{15} cm^{-2}

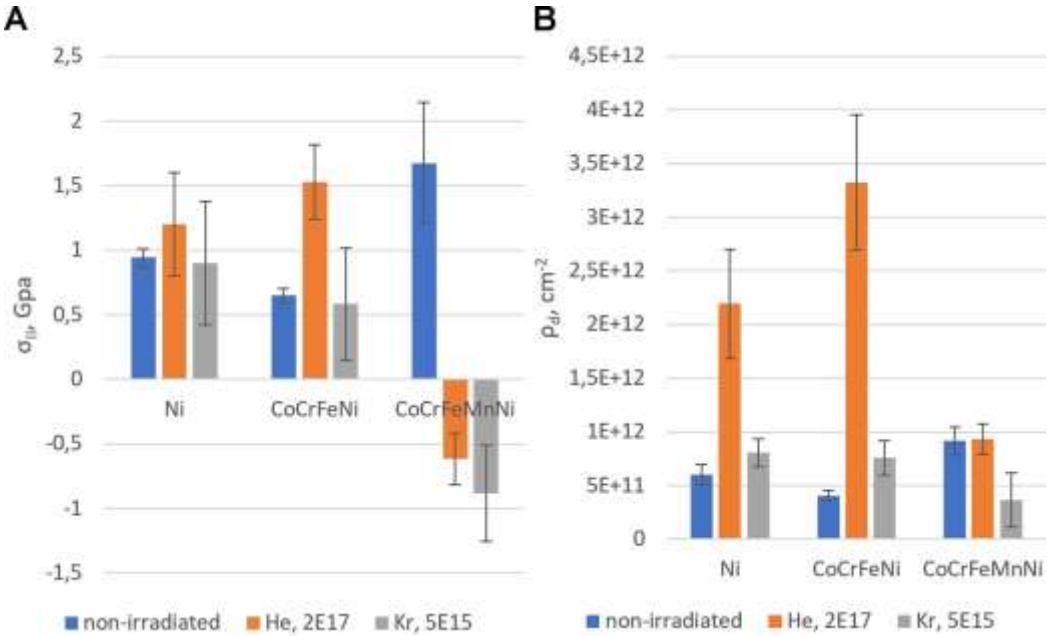

FIG. 8: Results of microstress and dislocation density estimations, obtained from XRD spectra using Williamson-Hall method for nonirradiated, He and Kr ion irradiated samples of pure Ni, CoCrFeMnNi and CoCrFeNi alloys: (a) microstress magnitudes; (b) dislocation density magnitudes

where c_i is an atomic concentration of i^{th} element, d_{ij} is the interatomic distance between atoms of i^{th} and j^{th} type in solid solution, n is the number of elements in solid solution (Lee et al., 2020).

The proposed version of lattice distortion parameter demands data about interatomic distances in solid solution, which are very hard to obtain, and also gives us an absolute magnitude of the atomic position deviations. Therefore this parameter can be simply modified to the following:

$$\frac{u^a}{\langle a \rangle} = \frac{u^a}{\sum_{i=1}^{n} c_i a_i}, \tag{4}$$

where a_i is the lattice constant of ith element in modification, when its lattice type equals the lattice type of solid solution examined, and for u^a calculation average lattice constants a_{ij} except d_{ij} is used in formulae (1–3). The parameter u^a is finally normalized on average lattice constant of the solid solution to characterize the magnitude of deformations and stresses of the lattice except absolute deviations magnitude.

Theoretical value of lattice distortions on alloys was estimated according to Eq. (4) using elemental composition data (Table 1), and information about FCC-modifications of all pure metals in system Co-Cr-Fe-Mn-Ni. Normalized lattice distortion parameter $u^a/\langle a \rangle$ has the value of 0.036 for CoCrFeMnNi HEA and 0.034 for CoCrFeNi MEA. For pure Ni, this quantity evidently equals 0. According to these data, one can expect irradiation superiority of CoCrFeMnNi HEA over CoCrFeNi, but the results of XRD shows at least insufficiency of such an estimation.

3. RESULTS AND DISCUSSION

Grain shape in all the researched samples may be conditioned by FCC-lattice and homogenization processes during technological annealing of the samples. Twins in the structure also may be formed by the mechanical cold-rolling processing. The drops and impurities on the surface are presumably the result of pollution and do not influence the properties of the samples.

The absence of visible changes of phase composition and significant radiation-induced element segregations in complex solid solutions may be due to the stability of the microstructure (Figs. 2 and 3). Blistering in pure Ni (Fig. 4) is caused by gas bubble aggregation and process of their deformation of the surface of the samples.

Diffraction reflex asymmetry is seen only in He-irradiated samples, while the symmetry of reflexes in nonirradiated and Kr-irradiated samples are not evidently disturbed (Figs. 5–7). It can be caused by additional microstresses in areas of maximum defect cluster and gas–vacancy cluster concentration. The absence of visible asymmetry in Kr-irradiated samples makes possible the dominant role of gas–vacancy clusters and gas bubbles in the process of creating the areas of greater microstresses, because gas-impurity concentration for He 2×10^{17} cm^{-2} irradiation is an order higher than Kr 5×15^{15} cm^{-2}, thus the damage dose in He is 2.5 times lower in comparison with Kr.

Crystalline size decrease for all He-irradiated samples is caused by the increase of total area for small-angle subcrystalline boundaries as a result of new irradiation-induced dislocation appearance and diffusion (Fig. 8B). The dislocation diffusion and their radiation annealing can be slowed down by large amount of helium–vacancy complexes, while after crypton irradiation the magnitude of dislocation density increase is much lower or negative than after helium irradiation. Being so, for CoCrFeMnNi HEA dislocation density seems to decrease significantly after Kr irradiation and shows very small increase in case of He irradiation. The mobility of dislocations in CoCrFeMnNi may be much greater in comparison with CoCrFeNi and pure Ni. Although

CoCrFeNi and pure Ni show the behavior, close to each other, the disorder with increased elastic modulus can slow the diffusion of dislocations in HEA, leading to greater increase of their density. Irradiation with He is likely to create large amount of free vacancies and gas–vacancy complexes, causing tension stresses in pure Ni and ternary CoCrFeNi HEA. However, the addition of Mn to CoCrFeNi can change the behavior of gas bubbles to the side of saving a large amount small bubbles, but suppression of void and bigger bubble aggregation. Mn is a fast-diffusive element which annihilates free vacancies by recombination mechanism. In Kr irradiation, less vacancies are occupied with gas, which results in greater amounts of annihilated vacancies and total increase of compressive stresses.

Normalized distortion parameter is an estimation of radiation resistance of the material in multicomponent solid-solution alloys. Main working rule "the more the distortion—the more the radiation resistance" can be verified by the superiority of HEAs compared with pure Ni. But this method of estimation seems to be quantitatively incorrect, because the real magnitude of crystal lattice distortion can differ from the results of calculations according to Eq. (4). Also the properties of the material depend first on particular chemical composition, and the distortion parameter accounts only the geometry of the lattice without its energy characteristics. This detail makes such an estimation variant primary (it helps to choose theoretically more radiation resistant alloy), but insufficient and uncomprehensive.

The result of normalized distortion parameter calculations is strongly dependent on stoichiometry of the calculated alloy (it can change greatly with rather small changes in elemental composition), that can help to vary elemental composition on design stage before depositing and researching particular materials, because optimal composition is not always equiatomic.

4. CONCLUSIONS

Main conclusions can be formulated as following:

1. Low energy ion irradiation resistance of three materials with FCC lattice was analyzed: pure Ni, CoCrFeNi MEA, and CoCrFeMnNi HEA. They were deposited by arc melting with sequential double annealing and cold rolling, having single-phase structure of solid solutions (complex alloys) and near equiatomic elemental composition.
2. Pure Ni has lower irradiation resistance than complex CoCrFeNi HEA and CoCrFeMnNi HEA. It shows blistering, while microstructure of complex alloys is stable after He 40 keV (2×10^{17} cm^{-2}) and Kr 280 keV (5×10^{15} cm^{-2}) irradiation. The changes in structural parameters of CoCrFeNi are greater, than in pure Ni HEA after ion irradiation because of better resistance of HEA to swelling. In case of CoCrFeMnNi, fast-diffusive element addition changes the behavior of the system to the side of creation of additional gas–vacancy complexes, causing additional compressive microstress.
3. Normalized distortion parameters can estimate comparative radiation resistance of HEAs according to the rule "The more the distortion—the more the radiation resistance." This estimation is useless in quantitative analysis, but may *a priori* help to choose theoretically more radiation resistant alloy from some compositions.

ACKNOWLEDGMENTS

This study was supported by State Program of Scientific Research "Energy and Nuclear Processes and Technologies" (2.1.03.2) and Tomsk State University Development Programme (priority 2030).

The authors are glad to thank the team of K. Jin from Beijing Institute of Technology, Beijing, China for performing the deposition of the objects and the team of A.E. Ryskulov from

Institute of Nuclear Physics, Nur-Sultan, Kazakhstan for collaboration in carrying out the ion irradiation experiment.

REFERENCES

Cantor, B., Chang, I.T.H., Knight, P., and Vincent, A.J.B., Microstructural Development in Equiatomic Multicomponent Alloys, *Mater. Sci. Eng.*, vol. **375**, pp. 213–218, 2004.

Jones, N.G. and Owen, L.R., Lattice Distortion in High-Entropy Alloys, *Encyclopedia of Materials: Metals and Alloys*, Amsterdam: Elsevier, 2020.

Karati, A., Guruvidyathri, K., Hariharan, V.S., and Murty, B.S., Thermal Stability of AlCoFeMnNi High-Entropy Alloy, *Scripta Mater.*, vol. **162**, pp. 465–467, 2019.

Koval, N.E., Juaristi, J.I., Muiño, R.D., and Alducin, M., Structure and Properties of CoCrFeNiX Multi-Principal Element Alloys from *Ab Initio* Calculations, *J. Appl. Phys.*, vol. **127**, Article ID 145102, 2020.

Lee, C., Chou, Y., Kim, G., Song, G., Gao, M.C., Zhang, C., Chen, W., Poplawsky, J., Chou, Y.C., Choo, H., and Liaw, P.K., Lattice-Distortion-Enhanced Yield Strength in a Refractory High-Entropy Alloy, *Adv. Mater.*, Article ID 2004029, 2020.

Li, W., Xie, D., Li, D., Zhang, Y., Gao, Y., and Liaw, P.K., Mechanical Behavior of High-Entropy Alloys, *Prog. Mater. Sci.*, vol. **118**, Article ID 100777, 2021.

Lu, Y., Huang, H., Gao, X., Ren, C., Gao, J., Zhang, H., Zheng, S., Jin, Q., Zhao, Y., Chenyang, L., Wang, T., and Li, T., A Promising New Class of Irradiation Tolerant Materials: $Ti_2ZrHfV_{0.5}Mo_{0.2}$ High-Entropy Alloy, *J. Mater. Sci. Technol.*, 2018. DOI: 10.1016/j.jmst.2018.09.034

Manzoni, A.M. and Glatzel, U., High-Entropy Alloys: Balancing Strength and Ductility at Room Temperature, *Encyclopedia of Materials: Metals and Alloys*, Amsterdam: Elsevier, 2020.

Murty, B.S., Yeh, J.-W., and Ranganathan, S., *High-Entropy Alloy*, 1st ed., Oxford, UK: Butterworth-Heinemann, 2014.

Pacheco, V., Lindwall, G., Karlsson, D., Cedervall, J., Fritze, S., Ek, G., Berastegui, P., Sahlberg, M., and Jansson, U., Thermal Stability of the HfNbTiVZr High-Entropy Alloy, *Inorg. Chem.*, vol. **58**, pp. 811–820, 2019.

Rogachev, A.S., Structure, Stability and Properties of High-Entropy Alloys, *Phys. Metals Metal Sci.*, vol. **121**, no. 8, pp. 807–841, 2020 (in Russian).

Senkov, O.N., Scott, J.M., Senkova, S.V., Miracle, D.B., and Woodward, C.F., Microstructure and Room Temperature Properties of a High-Entropy TaNbHfZrTi Alloy, *J. Alloys Compounds*, vol. **509**, pp. 6043–6048, 2011.

Son, S., Kim, S., Kwak, J., Gu, G.H., Hwang, D.S., Kim, Y.T., and Kim, H.S., Superior Antifouling Properties of a CoCrFeMnNi High-Entropy Alloy, *Mater. Lett.*, vol. **300**, Article ID 130130, 2021.

Song, H., Ma, Q., Zhang, W., and Tian, F., Effects of Vacancy on the Thermodynamic Properties of Co-Cr-Fe-Mn-Ni High-Entropy Alloys, *J. Alloys Compounds*, vol. **885**, Article ID 160944, 2021.

Tian, Y., Li, L., Li, J., Yang, Y., Li, S., and Qin, G., Correlating Strength and Hardness of High-Entropy Alloys, *Adv. Eng. Mater.*, Article ID 2001514, 2021.

Xea, S.Q., Wang, Z., Yang, T., and Zhang, Y., Recent Progress in High-Entropy Alloys, *J. Iron Steel Res.*, vol. **22**, pp. 879–884, 2015.

Ye, Y.F., Wang, Q., Lu, J., Liu, C.T., and Yang, Y., High Entropy Alloy: Challenges and Prospects, *Prog. Mater. Sci. Mater. Today*, pp. 1–14, 2015.

Yu, P.F., Zhang, L.J., Cheng, H., Zhang, H., Ma, M.Z., Li, Y.C., Li, G., Liaw, P.K., and Liu, R.P., The High-Entropy Alloys with High Hardness and Soft Magnetic Property Prepared by Mechanical Alloying and High-Pressure Sintering, *Intermetallics*, vol. **70**, pp. 82–87, 2016.

Zhang, Y., Zuo, T.T., Tang, Z., Gao, M.C., Dahmen, K.A., Liaw, P.K., and Lu, Z.P., Microstructures and Properties of High-Entropy Alloys, *Prog. Mater. Sci.*, vol. **6**, pp. 1–93, 2014.

Zhang, Z., Han, E.H., and Xiang, C., Effect of Helium Ion Irradiation on Short-Time Corrosion Behavior of Two Novel High-Entropy Alloys in Simulated PWR Primary Water, *Corrosion Sci.*, vol. **191**, Article ID 109742, 2021.